

See discussions, stats, and author profiles for this publication at: <https://www.researchgate.net/publication/15057639>

# Small Molecule Binding to an Artificially Created Cavity at the Active Site of Cytochrome c Peroxidase

ARTICLE *in* BIOCHEMISTRY · MAY 1994

Impact Factor: 3.02 · DOI: 10.1021/bi00179a004 · Source: PubMed

---

CITATIONS

100

---

READS

12

## 4 AUTHORS, INCLUDING:



Melissa Fitzgerald

Pfizer Inc.

16 PUBLICATIONS 397 CITATIONS

[SEE PROFILE](#)



Duncan E Mcree

The Scripps Research Institute

110 PUBLICATIONS 9,234 CITATIONS

[SEE PROFILE](#)

# Small Molecule Binding to an Artificially Created Cavity at the Active Site of Cytochrome *c* Peroxidase<sup>†,‡</sup>

Melissa M. Fitzgerald, Michael J. Churchill, Duncan E. McRee, and David B. Goodin\*

Department of Molecular Biology, MB8, The Scripps Research Institute, 10666 North Torrey Pines Road, La Jolla, California 92037

Received November 24, 1993; Revised Manuscript Received January 24, 1994®

**ABSTRACT:** In the oxidized “ES” state of cytochrome *c* peroxidase, Trp-191 is reversibly oxidized to a stable cation free radical by the hypervalent heme. To explore the potential for engineering a binding site for heterocyclic compounds at this site, the mutant W191G was constructed. Two independent crystal structures of W191G at 2.1- and 2.3-Å resolution show that W191G contains a well-defined, ~180-Å<sup>3</sup> cavity at the Trp-191 site. The cavity is occupied by five ordered water molecules which participate in an extensive hydrogen-bonding network with each other, with polar main-chain atoms, and with the carboxylate of Asp-235. After a number of heterocyclic compounds were screened, evidence was obtained that substituted imidazoles bind to the cavity of W191G. Titration of W191G with imidazole resulted in a perturbation of the Soret absorption band that was not observed for W191H, W191F, or the native enzyme. The dissociation constants for binding of benzimidazole, imidazole, 2-ethylimidazole, 1-methylimidazole, 2-methylimidazole, and 1,2-dimethylimidazole to W191G were respectively 2.58, 0.70, 0.36, 0.057, 0.047, and 0.027 mM at pH 6.0. The highest binding affinity was exhibited by 1,2-dimethylimidazole, indicating that steric interactions and the efficiency of filling the cavity are important determinants for specificity. The  $K_d$  for imidazole binding increased from 0.7 mM at pH 6 to 3.0 mM at pH 8 and could be fit to a single proton ionization curve with a  $pK_a$  of 7.4, demonstrating the preferential binding by the imidazolium ion ( $pK_a = 7.3$ ). The binding of a number of substituted imidazoles to the cavity of W191G was verified by X-ray crystallographic analysis. The most clearly defined density was observed for W191G crystals soaked in 1 mM 1,2-dimethylimidazole and was consistent with an oriented occupation in which the unsubstituted nitrogen forms a hydrogen bond or ion pair interaction with Asp-235. Thus, enhanced binding of positively charged molecules may be the result of interactions with this carboxylate. An analogous interaction may stabilize the developing positive charge on the Trp-191 radical of the wild-type enzyme. While the oxidation of imidazoles by the ferryl intermediate of W191G was neither expected nor observed, this study has defined the structural determinants for small molecule binding to an artificially created cavity near a heme center which is capable of generating oxidized species at a potential of over 1 V, and these results will guide future attempts for novel substrate oxidation by CCP.

An important goal of protein engineering would be realized by the production of heme enzymes which are capable of oxidizing a substrate of choice. The successful design of such catalysts would provide insight into the mechanism of heme enzyme function and would lay important groundwork for the creation of practically useful catalysts for synthesis, drug design, and bioremediation. The oxidative chemistry utilized by the iron center of cytochrome P<sub>450</sub>, nitric oxide synthase (NOS),<sup>1</sup> and many other heme enzymes represents a clear

example of a catalytic theme exploited by nature for widely different purposes. For many of these enzymes, an oxyferryl ( $\text{Fe}^{4+}=\text{O}$ ) species is proposed in the stereospecific epoxidation of unmodified alkenes (Ortiz de Montellano, 1986), the hydroxylation of arginine in the synthesis of nitric oxide (White & Marletta, 1992; Bredt et al., 1991), and a host of electron-transfer-mediated oxidations of small molecules ranging from halide ions to lignin (Dawson, 1988; Tien & Kirk, 1983). Substrate oxidation by heme enzymes proceeds by at least two distinct mechanisms that are influenced in part by the type of access provided to the hypervalent heme center by the protein. Heme monooxygenases such as P<sub>450</sub> and nitric oxide synthase (NOS) are believed to insert the ferryl oxygen into the substrate molecule (Ortiz de Montellano, 1986; Dawson, 1988; Kwon et al., 1990; Leone et al., 1991) and thus require access of the substrate to the distal heme face of the oxidized enzyme intermediates. Peroxidases, on the other hand, appear to oxidize substrates by electron transfer to the heme center (Saunders, 1973), and many studies have implicated substrate access to the heme edge as an important factor in controlling the specificity of these reactions (Sakurada et al., 1986; Thanabala et al., 1987; Ortiz de Montellano, 1987, 1992; Veitch & Williams, 1990; DePillis et al., 1991; Banci et al., 1993).

The oxidized state (compound ES) of the yeast enzyme cytochrome *c* peroxidase (CCP) contains a protein-based free radical which may be of considerable interest in the engineering

\* This research was supported by Grants GM41049 to D.B.G. and GM15733 to M.M.F. from the NIH.

† The crystallographic coordinates for the structures presented in this work have been deposited with the Protein Data Bank, Chemistry Department, Brookhaven National Laboratory, Upton, NY 11973, from which copies are available (entries 1CMP and 1CMQ).

‡ Author to whom correspondence should be addressed.

§ Abstract published in *Advance ACS Abstracts*, March 1, 1994.

1 Abbreviations: 1MeIm, 1-methylimidazole; 2MeIm, 2-methylimidazole; BzIm, benzimidazole; CCP, cytochrome *c* peroxidase; CCP-(MKT), cytochrome *c* peroxidase produced by expression in *Escherichia coli* containing Met-Lys-Thr at the N-terminus; CCP-CN, cytochrome *c* peroxidase-cyanide complex; cyt *c*, cytochrome *c*; DMIm, 1,2-dimethylimidazole; EPR, electron paramagnetic resonance; ES, the H<sub>2</sub>O<sub>2</sub> oxidized state of CCP; HRP, horseradish peroxidase; Im, imidazole; IPTG, isopropyl β-thiogalactopyranoside; MPD, 2-methyl-2,4-pentanediol; NOS, nitric oxide synthase; Tris, tris(hydroxymethyl)aminomethane; W191F, mutant in which Trp-191 is replaced by Phe; W191G, mutant in which Trp-191 is replaced by Gly; W191H, mutant in which Trp-191 is replaced by His.

of novel substrate oxidation by this enzyme. Heme peroxidases react in their resting ferric ( $\text{Fe}^{3+}$ ) state with  $\text{H}_2\text{O}_2$ , resulting in the oxidation of the heme by 2 equiv (George, 1952, 1953; Yonetani & Ray, 1965; Yonetani et al., 1966). Horseradish peroxidase exhibits an oxyferryl ( $\text{Fe}^{4+}=\text{O}$ ) center and a porphyrin  $\pi$ -cation radical in its oxidized intermediate compound I (Dolphin et al., 1971) which is used for the oxidation of a wide range of organic substrates including indoleacetic acid. The site of substrate interaction in HRP has been suggested to be near the 8-methyl group of the heme edge (Ator & Ortiz de Montellano, 1987; Ator et al., 1987; Sakurada et al., 1986). In contrast to most peroxidases, CCP contains a tryptophan (Trp-191) on the proximal side of the heme near the 8-methyl group, and this residue is efficiently and reversibly oxidized to a free radical state in compound ES (Sivaraja et al., 1989; Scholes et al., 1989; Erman et al., 1989). Trp-191 participates in hydrogen bonding with the functionally important Asp-235, which in turn hydrogen bonds with the proximal heme ligand His-175 (Finzel et al., 1984). These interactions may provide a mechanism for oxidizing Trp-191, rather than Trp-51, on the distal heme face (Goodin & McRee, 1993).

It may prove more feasible to introduce new substrate specificity into a heme enzyme than for those enzymes which lack a prosthetic group. In general, the critical positioning of substrate near the catalytic residues and the sensitivity of the transition state to small changes in geometry provide a formidable barrier to rational design goals (Wells & Fersht, 1985; Knowles, 1987). However, for heme enzymes, much of the catalytic framework preexists within the heme and its immediate environment, and the type of chemistry observed may in large part be controlled by how substrates are given access to this center (Ortiz de Montellano, 1992). Indeed, the surrounding protein in many of these enzymes may serve as much to restrict heme access to unintentional substrates as to provide empowering interactions. Nevertheless, the successful introduction of a specific substrate binding site for a predetermined target molecule represents a significant challenge, requiring close control over protein structure, substrate–protein interactions, and electronic coupling between substrate and the catalytic center. We considered that the replacement of the Trp-191 free radical center by a significantly smaller residue might generate a cavity with shape and H-bond complementarity appropriate for the binding of small heterocyclic molecules. Cavity formation within the interior of proteins has been shown to be a feasible design goal. A number of mutants of T4 lysozyme contain buried cavities, some of which (L99A for example) are stabilized by binding hydrophobic probes such as benzene (Eriksson et al., 1992a,b, 1993). However, the utility of these observations as an enzyme design principle is uncertain, because other factors such as the solvent occupation and access of ligands to the cavity are expected to contribute to the specificity of ligand binding. In this paper we present a significant step toward these goals by documenting a well defined,  $\text{H}_2\text{O}$ -containing cavity at the free radical site of CCP. The cavity is shown to bind a series of substituted imidazoles with high affinity and with parameters that can be readily understood in terms of substrate–protein interactions.

## MATERIALS AND METHODS

**Protein Expression and Purification.** CCP was overexpressed in *Escherichia coli* using the plasmid pT7CCP in which expression was placed under the control of T7 RNA polymerase. The plasmid was constructed from the plasmid

pLACCCP2-8 (Goodin et al., 1991) by replacing the lac promoter with the T7 promoter utilizing sticky foot mutagenesis (Clackson & Winter, 1989). CCP(MKT) refers to the protein produced from the cloned gene and contains Met-Lys-Thr at the N-terminus (Goodin et al., 1991). It is also distinguished from the protein isolated from baker's yeast by containing Ile-53 and Gly-152 (Kaput et al., 1982). Mutants of cytochrome *c* peroxidase were constructed by site-directed mutagenesis (Ner et al., 1988a; Kunkel et al., 1991) and verified by dideoxy DNA sequencing (Ner et al., 1988b). High-level expression of the apoprotein was achieved in *E. coli* BL21(DE3) (Studier et al., 1990). Cultures were grown in rich media (containing, per liter, 10 g of bactotryptone, 8 g of yeast extract, 5 g of NaCl, 1 mL of glycerin, and 100 mg of ampicillin) at 37 °C for 12 h, induced with IPTG (added to make 0.5 mM), and harvested at 15 h. High yields of W191G apoprotein were also obtained without induction by IPTG, by growing the cultures for 30 h in a super broth media (containing, per liter, 12 g of bactotryptone, 24 g of yeast extract, 2.3 g of  $\text{KH}_2\text{PO}_4$ , 12.5 g of  $\text{K}_2\text{HPO}_4$ , and 100 mg of ampicillin). The apoprotein was prepared, reconstituted with heme, and purified as described previously (Goodin et al., 1991). Purified enzyme was recrystallized twice from distilled water and stored as a crystal suspension at 77 K. For use, crystals were washed in cold distilled water and dissolved in the appropriate buffer. Protein concentrations were determined from the molar absorptivities ( $\epsilon_{408}^{\text{CCP(MKT)}} = 101 \text{ mM}^{-1} \text{ cm}^{-1}$ ;  $\epsilon_{412}^{\text{W191G}} \approx \epsilon_{412}^{\text{W191H}} = 104 \text{ mM}^{-1} \text{ cm}^{-1}$ ;  $\epsilon_{410}^{\text{W191F}} = 106 \text{ mM}^{-1} \text{ cm}^{-1}$ ) as determined from the pyridine hemochromogens (Nicola et al., 1975).

**Binding Measurements.** Probe compounds were obtained from Sigma or Janssen Chimica. Binding assays were performed by difference absorption spectral titrations using a Hewlett-Packard 8452A diode-array spectrophotometer. Stock solutions of imidazole (1.0 M) and its methyl-substituted derivatives (0.1 M) were prepared in  $\text{H}_2\text{O}$  and adjusted to the same pH as the protein buffer with  $\text{H}_3\text{PO}_4$ . The 2-ethylimidazole and benzimidazole stock solutions (1.0 M) were prepared in methanol. Stock protein solutions were diluted into 3.0 mL of the stated buffer, to give an absorbance of 1.0 at the Soret maximum. The protein solution was allowed to equilibrate at 20 °C for 30 min in the spectrophotometer with stirring, and the instrument was blanked. A 1- $\mu\text{L}$  aliquot of the test compound stock solution was added to the cuvette, and the difference absorption spectrum was recorded after the change in absorbance had equilibrated (usually 1 min). Dissociation constants were determined from Scatchard plots based on the difference absorbance at the Soret maximum, assuming one binding site per protein molecule.

**Steady-State Kinetics and Stability Measurements.** The rate of W191G-catalyzed oxidation of reduced horse heart cytochrome *c* (cyt *c*) by  $\text{H}_2\text{O}_2$  was determined as previously described for CCP(MKT) (Goodin et al., 1987, 1991), except that the concentration of W191G in the assay was increased to 250 nM, due to the relative unreactivity of the mutant toward cyt *c* oxidation. Kinetic determinations were carried out at 22 °C in 20 mM Tris/phosphate (pH 6.0), 25  $\mu\text{M}$  reduced cyt *c*, and 10–100  $\mu\text{M}$   $\text{H}_2\text{O}_2$ .

Thermal denaturation profiles for CCP(MKT) and W191G were measured by optical difference spectroscopy using a Hewlett-Packard 8452A diode-array spectrophotometer. Approximately 10  $\mu\text{M}$  protein in 0.1 M potassium phosphate buffer was equilibrated at the starting temperature [15 °C for CCP(MKT) and 12 °C for W191G]. The spectrophotometer was blanked, and the sample temperature was raised

Table 1: Data Collection and Refinement Statistics<sup>a</sup>

	W191G	W191G	W191H	W191G soaked in			
	W191G	W191G	W191H	Im	1MeIm	2MeIm	DMIm
Data Collection							
crystal form <sup>b</sup>	MKT	yeast	MKT	yeast	MKT	MKT	MKT
unit cell	105.2	107.6	105.9	107.8	105.0	104.7	104.8
<i>a</i> , <i>b</i> , <i>c</i> (Å)	74.2	76.8	74.3	77.2	73.9	73.9	74.0
	45.1	51.6	45.0	51.7	45.2	45.3	45.3
resolution (Å)	2.0	2.1	2.0	2.1	1.9	1.9	1.9
<i>I</i> / <i>σ<sub>I</sub></i> (av)	15.8	19.3	18.6	16.3	25.2	21.3	21.8
<i>I</i> / <i>σ<sub>I</sub></i> (last shell)	1.7	2.8	1.5	1.5	1.9	2.2	2.0
no. of reflections	19881	20478	17773	16612	21369	16651	22020
completeness (%)	80	79	73	64	74	58	76
<i>R</i> <sub>sym</sub>	0.057	0.044	0.068	0.077	0.049	0.044	0.054
Refinement							
<i>R</i>	0.19	0.18	0.18	0.19	0.20		0.19
resolution (Å)	2.3 <sup>c</sup>	2.1	2.0	2.1	1.9		1.9
no. of waters	55	105	50	50	50		50

<sup>a</sup> Data were collected at 15 °C on a Siemens 3 axis camera/area detector using Cu K $\alpha$  radiation and processed as described earlier (Goodin & McRee, 1993). Each data set was collected on a single crystal, and *R*<sub>sym</sub> represents the agreement between  $F_o$  for equivalent reflections. Values of *I*/*σ<sub>I</sub>* (last shell) represent the average *I*/*σ<sub>I</sub>* for the 10% of the data of highest resolution. The indicated number of observed waters was included in the final refinement, and the *R* values give the crystallographic residuals for the observed and model-derived structure factor amplitudes. W191G crystals were soaked in 10 mM imidazole (Im), 1 mM 1-methylimidazole (1MeIm), 1 mM 2-methylimidazole (2MeIm), 1 mM 1,2-dimethylimidazole (DMIm), or 10 mM benzimidazole (BzIm). <sup>b</sup> Crystals of W191G were obtained in two forms which differ in crystal packing within the unit cell and can be distinguished by the unit cell dimensions [see text and Wang et al. (1990)]. <sup>c</sup> Data were 91% complete to this resolution.

at a rate of 2°/min while absorption spectra were collected. The fraction of unfolded protein was calculated from the difference absorption data to obtain *T<sub>m</sub>*.

**X-ray Crystallographic Analysis.** Single crystals of X-ray diffraction quality were grown from 25% 2-methyl-2,4-pentanediol (MPD) by vapor diffusion (Wang et al., 1990). W191G crystals were soaked for 12 h in the test compounds (12 mM imidazole, 10 mM benzimidazole, 1 mM 1-methylimidazole, 1 mM 2-methylimidazole, or 1 mM 1,2-dimethylimidazole) in 27% MPD and 30 mM sodium phosphate buffer, pH 6.0. X-ray diffraction data were collected at 15 °C using Cu K $\alpha$  radiation from the rotating anode of a Rigaku X-ray generator and a Siemens area detector. Data were analyzed by difference Fourier techniques using the Scripps XtalView software (McRee, 1992) and molecular models refined using XPLOR (Brünger et al., 1987).

## RESULTS

**W191G Leaves a Cavity Occupied by Ordered Solvent.** Using site-directed mutagenesis, we have replaced Trp-191 with several residues, including W191G, W191F, and W191H. Each of these mutant proteins has been produced in *E. coli* by established procedures and can be reconstituted with heme and crystallized. Crystals of W191G were obtained in two different crystal forms that have been described previously (Wang et al., 1990). We refer to these as the “MKT” form, preferred by the *E. coli* produced protein, and the “yeast” form, which was first observed for the protein purified from baker’s yeast. These two enzymes differ in sequence at the three N-terminal residues and at two internal positions as previously noted (Goodin et al., 1991; Wang et al., 1990). Both crystal forms belong to the same space group (*P*2<sub>1</sub>2<sub>1</sub>2<sub>1</sub>) and differ in unit cell parameters, with *a* = 105.2 Å, *b* = 74.3 Å, and *c* = 45.4 Å for the MKT form, and *a* = 107.6 Å, *b* = 76.8 Å, and *c* = 51.6 Å for the yeast form. The structures have been observed to differ primarily in the way the protein monomers are packed within the asymmetric unit (Wang et al., 1990).

In order to evaluate subtle effects that may arise from differences in crystal packing on our subsequent analysis of the cavity and its occupation, we have solved the structures

of W191G in both crystal forms (see Table 1). Examination of  $F_{\text{mutant}} - F_{\text{MKT}}$  difference Fourier maps constructed from the structure factors of the wild-type protein CCP(MKT) (Goodin & McRee, 1993) indicated the loss of density for Trp-191 and very little change in the surrounding protein structure. Thus, models were constructed by removal of the Trp-191 side chain from the CCP(MKT) structure, and these models were refined against the data using geometry-restrained least squares refinement with XPLOR (Brünger et al., 1987) (see Table 1). The structure of W191G in the vicinity of residue 191 is shown in Figure 1A for both crystal forms. Each of the two structures was quite similar (RMS differences were 0.49 Å for all atoms and 0.23 Å for C<sub>α</sub> atoms). We also observe very little change in the conformation of the protein as compared to wild type, including Asp-235 and the His-175 heme ligand. In the native protein, the buried Asp-235 accepts a hydrogen bond from both the His-175 ligand and the indole NH of Trp-191, and this linkage has been shown to be critical in the control of the Trp-191 orientation (Wang et al., 1990) and in the electronic coupling between the Trp-191 free radical and the heme (Goodin & McRee, 1993). The only significant changes in the surrounding protein structure are near position 191, in which the main chain moves 0.5 Å away from the cavity created by removal of Trp-191, and in the main chain near His-175 resulting from a small movement of His-175 toward the heme iron. As shown in Figure 1A, these small movements are reproduced in each of the two independently determined structures of this mutant. The side chain of Trp-191 is completely buried, so the absence of structural rearrangements upon its replacement by Gly implies that a buried cavity exists in W191G. The solvent-accessible surface calculated from the refined model of W191G using a 1.4-Å probe (Connolly, 1983) is shown in Figure 1B. Also shown inside this surface is the surface representing the probe sphere centers (yellow). The observed cavity volume was calculated by creating a fine 0.1-Å grid that covered the region of the cavity. The grid points that were outside the solvent-accessible surface were removed, and the volume was determined by the number of enclosed grid points. For W191G, a small finger-like extension (smaller than a 1.4-Å probe) in the solvent-accessible surface of the cavity was manually blocked by adding

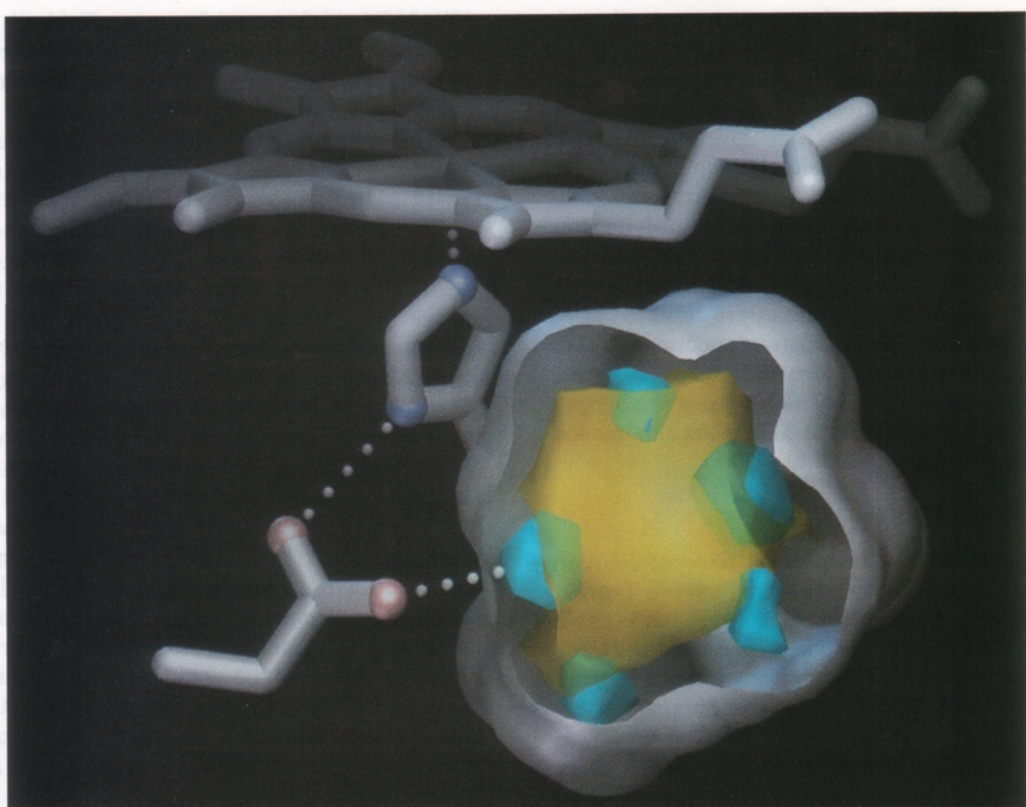
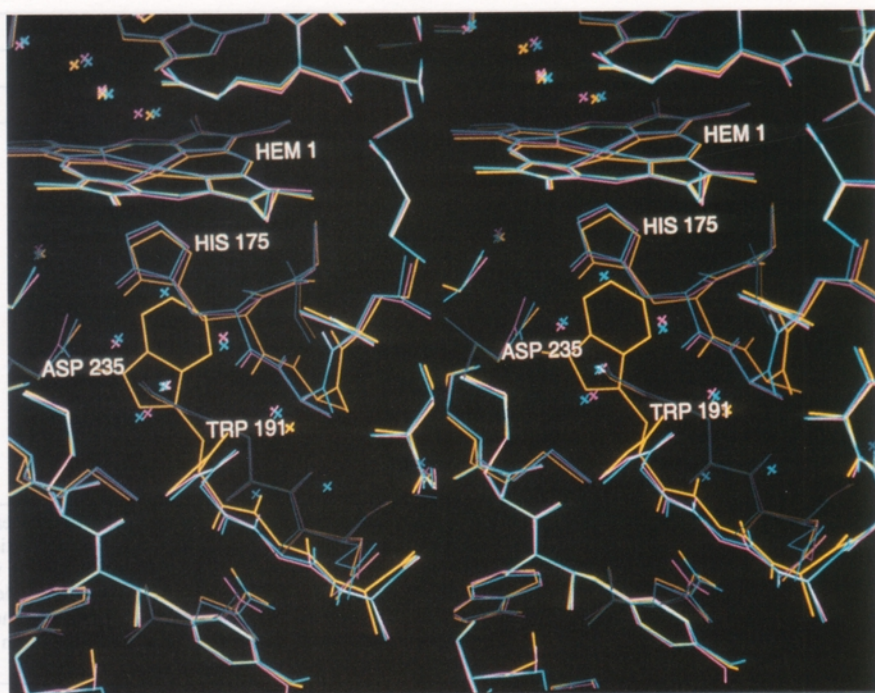


**FIGURE 1:** (A, top) Stereoviews of the refined models for W191G in the MKT crystal form (violet) at 2.3-Å resolution and in the yeast crystal form (blue) at 2.1-Å resolution overlaid on the model of the wild-type enzyme CCP(MKT) (yellow) at 1.8-Å resolution. (B, bottom) Solvent-accessible surface of the W191G cavity (gray) calculated using a 1.4-Å probe sphere (Connolly, 1983). This surface is cut away to display an inner surface (yellow) which represents the centers of the probe spheres used to calculate the outer surface. Also shown is the electron density for waters observed within the cavity (blue) obtained by contouring the omit map density of W191G in the MKT crystal form at  $4\sigma$ . The waters are positioned such that they roughly bisect the inner yellow surface, indicating that they are attached to the inside walls of the cavity.

an artificial water to the structure during the calculation. The observed cavity volume of W191G was  $182 \text{ \AA}^3$ . This is equal within experimental error to the value of  $188 \text{ \AA}^3$  predicted by replacing Trp-191 with Gly-191 in a molecular model using the structure of CCP(MKT) and assuming no change in the surrounding protein.

We have examined the state of occupation of the W191G cavity and observe that it contains five ordered solvent molecules. A model for W191G which included observed water molecules except for those within the cavity was first refined against the data until the  $R$  value had converged. Omit maps ( $F_o - F_c$ ) constructed from the refined structure

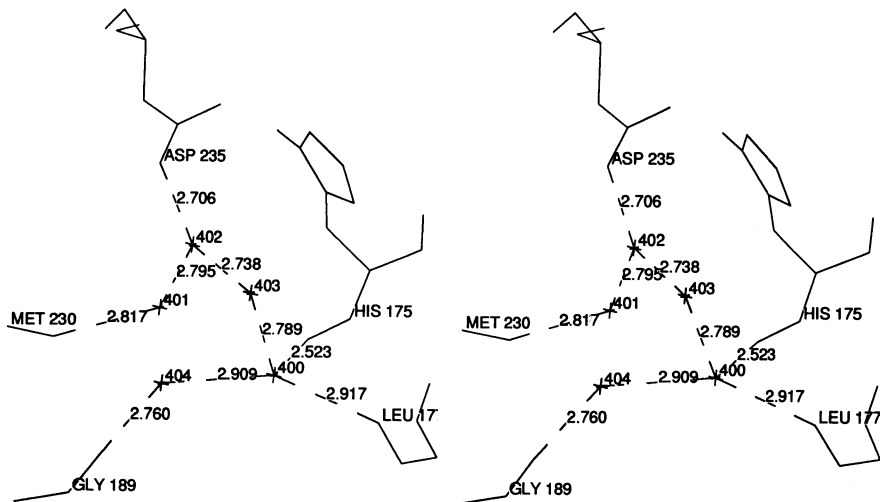


**FIGURE 2:** Stereoview showing the interactions between water molecules (indicated by cross marks numbered 400–404) occupying the W191G cavity. The view is from the direction of the heme plane, looking down on the His-175 ligand from the distal side. The distances for potential hydrogen-bonding interactions involving the water molecules are shown along the dashed lines. The peptide carbonyls of His-175, Leu-177, Met-230, and Gly-189 accept hydrogen bonds from the indicated water molecules. A hydrogen bond of unknown donor/acceptor status is indicated between the carboxylate of Asp-235 and HOH-402. Hydrogen bonds link the water molecules together in a continuous chain, ordered 401–402–403–400–404. Water 403 is not observed to make an interaction directly with the protein. Refined *B* values of waters 400–404 are respectively 7.7, 14.4, 15.9, 22.2, and 21.6 for the MKT crystal form and 9.7, 20.6, 19.2, 27.1, and 17.4 for the yeast crystal form.

factors showed the presence of five well-resolved electron density peaks. These peaks are represented for the MKT crystal form of W191G in Figure 1B (in blue) and are also presented below for the yeast crystal form in Figure 6A. Very similar peaks were observed for the two independently determined structures, demonstrating that the solvent occupation is both reproducible and not sensitive to subtle differences deriving from changes in crystal contacts and packing. Each of the five water molecules, numbered 400–404, are attached to the inside walls of the cavity. This is indicated in Figure 1B in which the electron density peaks (shown in blue) are observed to approximately bisect the cavity surface representing the probe atom centers (shown in yellow). As shown in Figure 2, an extensive network of hydrogen bonds both among the five waters and between these molecules and the cavity walls can be modeled. The cavity of W191G is far from hydrophobic, with several carbonyls of the main chain forming its surface. HOH-403 is the only one of the five that is not observed to interact with at least one polar atom in the protein, and as noted in Figure 2, this water has the highest refined *B* value of the five. Thus, the protein can accept hydrogen bonds from HOH-400 at the peptide carbonyls of His-175 and Leu-177, from HOH-401 at the peptide carbonyl of Met-230, and from HOH-404 at the carbonyl of Gly-189. In addition, a hydrogen bond of unknown donor/acceptor status may occur between HOH-402 and the carboxylate of Asp-235. This water occupies nearly the same position as the indole nitrogen of Trp-191 which donates a hydrogen bond to Asp-235 in the native enzyme. In addition to these water-protein interactions, a continuous chain of hydrogen bonds linking the water molecules together in the order 401–402–403–400–404 can be assigned. Additional weaker interactions between the five water molecules may also exist but have not been shown in Figure 2 because of poor geometry or an interatom distance of  $>3.1 \text{ \AA}$ . Several of the observed angles deviate significantly from the ideal  $109^\circ$  tetrahedral geometry. An example is noted for HOH-402, where the 401–402–403 angle is nearly tetrahedral ( $116.5^\circ$ ), but the angles between the Asp-235 oxygen and either HOH-401 or HOH-403 ( $84.3^\circ$  and  $156.3^\circ$ , respectively) do not approximate the ideal tetrahedral arrangement. This may imply a considerable

dynamic fluctuation in the network, in which HOH-402 may be viewed as either hydrogen bonded to both HOH-401 and HOH-403 or hydrogen bonded to Asp-235 alone. Finally, we note that although we have modeled the five electron density peaks in the W191G cavity as water molecules, we cannot exclude the possibility that one or more of these peaks are due to ion binding. This is particularly true of "HOH-402", which is positioned near Asp-235, and thus may represent cation binding at this site.

**Binding of Probe Molecules to the Cavity of W191G.** We have investigated the binding of a number of small heterocyclic molecules to the cavity of W191G. Indoles were considered the most obvious candidates, considering the shape and hydrogen bond complementarity provided by removal of Trp-191. However, a number of attempts to induce spectroscopic changes in the heme Soret upon soaking or reconstituting the W191G mutant proteins in the presence of indole, 3-methylindole, 5-hydroxyindole, or serotonin have provided inconclusive results. In addition, as described below, only small changes in the cavity occupation have been observed in several crystallographic experiments with indole-treated samples.

In sharp contrast to the results observed with indoles, we find clear evidence for the specific binding of imidazole derivatives within the W191G cavity. Titration of W191G with imidazole at pH 6 produces a significant effect on the heme Soret band (Figure 3C), which is not observed for CCP-(MKT) (Figure 3A), W191F (data not shown), or W191H (Figure 3B). The difference titration spectra of Figure 3 show that imidazole binding to W191G results in a 2–3% intensification of the Soret band. The difference peak maximum varies from 406 to 418 nm, depending on buffer and sample pH. At pH 6, the *K*<sub>d</sub> for binding of imidazole to W191G is  $0.70 \pm 0.09 \text{ mM}$  (see Figure 4A and Table 2). The mutant W191H should serve as an excellent control for the properties of a covalently bound, fully occupied imidazole in the cavity. We thus expect that the change in the optical spectrum of W191G induced upon imidazole binding within the cavity should be similar to the difference spectrum of the two mutants (W191H minus W191G). The observed difference spectra (spectra C and D of Figure 3, respectively) are indeed remarkably similar.

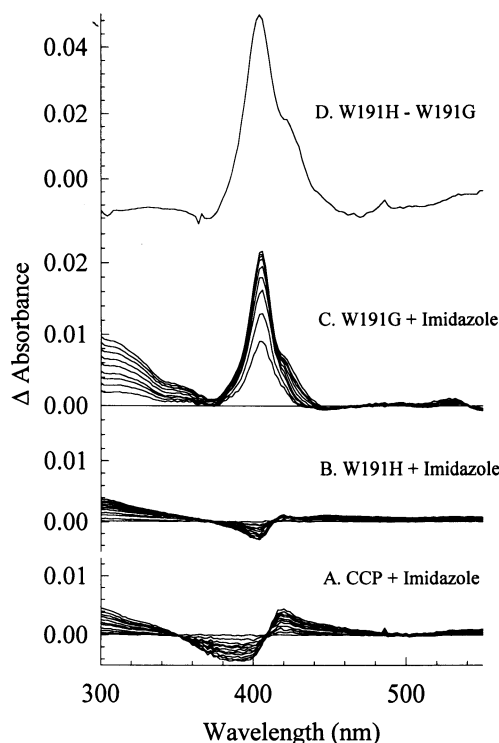


FIGURE 3: Optical difference spectra obtained by titration of CCP (MKT) (A), W191H (B), and W191G (C) with imidazole. Enzyme solutions (3 mL at  $\sim 10 \mu\text{M}$  in 0.1 M potassium phosphate, pH 6.0) were titrated at 20 °C with 1- $\mu\text{L}$  additions of 1.0 M imidazole, pH 6. The difference spectrum between W191H and W191G shown in (D) (obtained by subtraction of the normalized spectra of the two mutants in the absence of imidazole) is compared with the difference spectrum in (C) for the titration of W191G with imidazole.

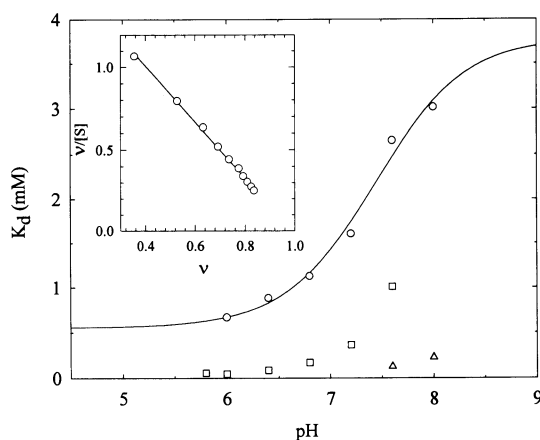


FIGURE 4: pH dependence of the dissociation constant  $K_d$  for the binding of imidazole (412 nm, O) or 2-methylimidazole (406 nm, □; 430 nm, Δ) to W191G, based on difference absorption spectral titrations. The solid line is the least squares fit of the imidazole data to a single proton ionization curve to give a  $pK_a$  value of 7.4, which is close to the  $pK_a$  of 7.3 for imidazole in solution. This indicates that the cavity preferentially binds the ionized imidazole. In the titration of W191G with 2-methylimidazole, an alkaline transition in the protein with a  $pK_a$  of 7.6 precluded the completion of the curve. Inset: Representative Scatchard plot utilized to obtain  $K_d$  at pH 6.0 from the difference absorbance ( $\Delta\text{Abs}$ ) at 412 nm in the titration of W191G with imidazole. The fractional occupation  $\nu$  was determined by extrapolating  $1/\Delta\text{Abs}$  vs substrate concentration  $[S]$  to infinite  $[S]$  and assuming one binding site.

The observed effect of imidazole on the spectra of W191G is not due to imidazole binding to the heme iron. First, the effects of imidazole on the wild-type protein are distinct from those on W191G. Imidazole titration of wild-type CCP (MKT) results in a much smaller (<0.5%) change in the

Table 2: Dissociation Constants for Binding of Substituted Imidazoles to W191G at pH 6<sup>a</sup>

compound	$K_d$ (mM)	$pK_a$
imidazole	$0.70 \pm 0.09^b$	7.0, 7.3
W191G-CN + imidazole	0.40	
1-methylimidazole	0.057	7.3, 7.33
2-methylimidazole	0.047	7.6, 7.9
1,2-dimethylimidazole	0.027	7.9
2-ethylimidazole	0.36	8.0
benzimidazole	2.58	5.5

<sup>a</sup> Values of  $K_d$  were determined by linear regression of Scatchard plots,  $\nu/[S]$  vs  $\nu$ , where  $\nu$  is the fractional occupation and  $[S]$  is the small molecule concentration. Fractional occupation was determined by extrapolating  $1/\Delta\text{Abs}$  vs  $1/[S]$  to infinite  $[S]$  and assuming one binding site per protein. In each case, imidazole titration of control proteins (W191H or W191F) gave very small changes in  $\Delta\text{Abs}$  that did not saturate or give linear Scatchard plots. Also shown are reported values of the  $pK_a$  for each imidazole (Katritzky & Rees, 1984). <sup>b</sup> Standard deviation of five independent determinations. Other uncertainties are estimated to be  $\pm 10\%$ .

spectrum that is associated with a red shift of the Soret band (Figure 3A). Second, imidazole titration of the W191G–cyanide complex (protein:CN<sup>-</sup> = 1:200, pH 6) causes a 2–3% perturbation of the Soret with a dissociation constant for imidazole of 0.40 mM (Table 2). The similar binding behavior of W191G and the W191G–CN<sup>-</sup> complex demonstrates that cyanide binding does not interfere significantly with binding of imidazole. Finally, no perturbation is observed in the crystal structure of the distal heme cavity of W191G in the presence of 12 mM imidazole as shown below.

**Effect of Imidazole Substituents on Binding Specificity.** We have examined the effect on W191G binding with varying imidazole substituents to obtain information about the steric limitations within the cavity. We find that methyl groups significantly increase the binding affinity of the imidazoles but that larger substituents are not well tolerated. As shown in Table 2, the values of  $K_d$  for binding of 1-methylimidazole and 2-methylimidazole to W191G at pH 6 (0.057 and 0.047 mM, respectively) are at least 10-fold lower than that observed for imidazole (0.70 mM). For 1,2-dimethylimidazole, we observe a  $K_d$  of 0.027 mM, which represents the tightest binding probe that we have found to date. We note that the effect of adding two successive methyl groups is additive, and this may reflect increasing hydrophobic interactions resulting from more efficient filling of the cavity. However, the limit of this effect is readily exceeded, as the  $K_d$  for binding of 2-ethylimidazole is 0.36 mM. This  $K_d$  is lower than that observed for imidazole itself but is significantly larger than the values for the methylimidazoles.

**Binding Is Specific for the Imidazolium Ion.** As discussed above, the buried carboxylate of Asp-235 forms part of the cavity wall and is observed to hydrogen bond to Trp-191 in the wild-type enzyme. This observation suggests that positively charged molecules might form particularly favorable interactions within the cavity. This hypothesis was verified by demonstrating that the imidazolium ion is more strongly bound to the cavity than is neutral imidazole. Figure 4 shows that the  $K_d$  for imidazoles binding to W191G drops significantly as the pH is reduced from 8 to 6. The variation of  $K_d$  with pH can be fit to a single proton ionization curve (see Figure 4) with a  $pK_a$  of 7.4, which is very close to the observed  $pK_a$  of 7.3 for imidazole in solution. The fit to the data of Figure 4 indicates that  $K_d$  for binding of the imidazolium ion (0.55 mM) is approximately 10 times lower than that for neutral imidazole (3.8 mM). The pH dependence for the binding of 2-methylimidazole is also consistent with the preferential

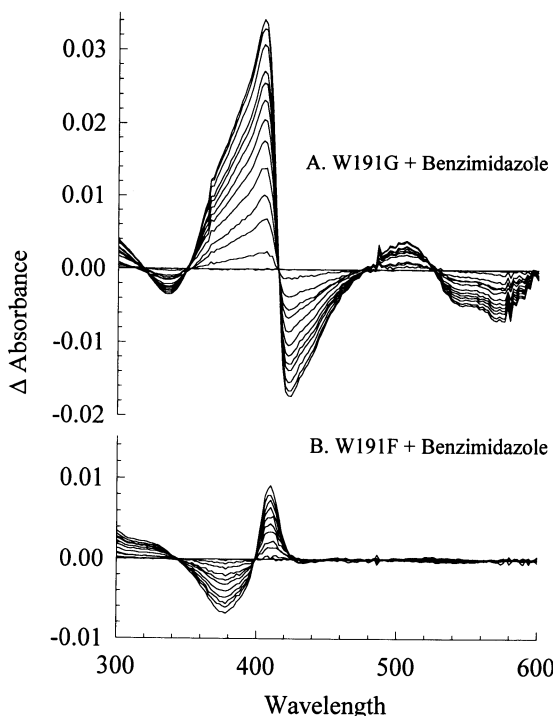


FIGURE 5: Optical difference spectra at pH 6 for W191G (A) and W191F (B) titrated with successive 1- $\mu$ L additions of 1.0 M benzimidazole in methanol at 20 °C. The titrations were performed as described in Figure 3. A least squares fit of the data gave  $K_d$  = 2.58 mM.

binding by the ionized imidazolium as indicated in Figure 4. In this case the  $K_d$  also increases as the pH is raised to the  $pK_a$  for 2-methylimidazole (7.9). Unfortunately, as the pH is raised beyond 7.5, we observe a transition in the optical difference spectra and a second binding constant appears, as shown by the squares of Figure 4. This may reflect an alkaline transition that has been previously reported at  $pK_a$  = 7.6 for several mutants of CCP in which the proximal hydrogen-bonding network is interrupted (Smulevich et al., 1988; Vitello et al., 1992; Goodin & McRee, 1993). This protein-based transition precludes the completion of the  $K_d$  vs pH curve for 2-methylimidazole. The initial portion of the curve is, however, consistent with the slightly higher  $pK_a$  of 7.9 for 2-methylimidazole relative to imidazole.

In view of the above results, we considered the possibility that indoles were not observed to strongly bind to the W191G cavity, not because of their size but because they lack the positive charge determinant. The structurally similar molecule benzimidazole has  $pK_a$  = 5.5 and thus would exist in a charged state to a significant degree at pH 6. Unlike the results for the neutral indoles, we observe that benzimidazole induces a significant perturbation on the optical spectra of W191G (Figure 5) that indicates a partial shift from the low-spin to the high-spin state. These data follow a characteristic binding isotherm to give a  $K_d$  of 2.58 mM at pH 6. A much smaller perturbation of a completely different nature is observed for the control protein W191F which is approximately linear with the concentration of benzimidazole up to 10 mM and thus represents very weak binding or nonspecific perturbation on the spectrum.

**Structural Characterization of Imidazole Binding.** We have obtained crystallographic structural characterization to verify the spectroscopic evidence for binding of imidazoles to the cavity of W191G and to characterize the mode and orientation of bound probe molecules. We have thus collected a number of X-ray diffraction data sets as described in

Materials and Methods on crystals of W191G soaked in mother liquor containing various probe molecules. Such trials have included imidazole, 1-methylimidazole, 2-methylimidazole, 1,2-dimethylimidazole, benzimidazole, benzene, indole, 3-methylindole (skatole), 5-hydroxyindole, and 5-hydroxytryptamine (serotonin).

Fourier difference maps were examined for each of the above soaks, and the results are in full agreement with the spectroscopic data which indicate binding of imidazoles but not of the larger hydrophobic probes. Very little perturbation is observed in the structure of the water molecules of the cavity for crystals soaked in indole or its derivatives at concentrations up to 5 mM (data not shown). However, significant perturbations were observed in such maps for crystals soaked in imidazole derivatives. To examine the state of occupation of the cavity under these conditions, a series of omit maps were constructed and are presented in Figure 6. These maps were calculated as  $F_o - F_c$ , where  $F_c$  represents the structure factors derived from the model for W191G refined without any atoms represented in the cavity. The maps thus represent the electron density present in the cavity arising from solvent or probe molecule occupation. The five clearly resolved water molecules observed in the unsoaked omit map of Figure 6A are replaced by two electron density peaks upon soaking in 12 mM imidazole (Figure 6B). One of these peaks is well represented by the position of HOH-401 of W191G, and the other larger disk-shaped peak replaces the other four water molecules. By placing an imidazole model at the center of this second region of density, we find that the distance between atoms on the imidazole and the remaining water would be approximately 2.5 Å and may thus be appropriate for a hydrogen bond. The omit map for W191G soaked in 1 mM 1-methylimidazole is shown in Figure 6C, in which a single large disk of electron density is observed. Several minor protrusions are evident on this density which may represent the methyl group in several conformations. However, these features may also be explained by partial occupancy of the water molecules of the empty cavity, if we interpret the density as representing a time-averaged structure in which either a probe molecule or solvent occupies the cavity in a mutually exclusive manner. A similar observation is made in Figure 6D for W191G soaked in 1 mM 2-methylimidazole. This density is much like that observed for imidazole. The highest affinity probe observed by spectroscopic measurements, 1,2-dimethylimidazole, also gives the clearest omit map and is shown in Figure 6E. This map, obtained from crystals soaked in 1 mM 1,2-dimethylimidazole, exhibits a clearly delineated disk of density with two prominent protuberances. While we cannot rule out the possibility that these features are due to residual occupation by solvent, the positions of the "ears" with respect to the main disk of density strongly suggest that they represent the two methyl substituents. In addition, such an assignment would leave the unsubstituted nitrogen of the ring in perfect position to make a hydrogen bond or ion pair interaction with Asp-235. Finally, we observe that soaking crystals in 10 mM benzimidazole causes only small changes in electron density within the cavity compared with unsoaked crystals (data not shown). This result may be the consequence of very weak binding, as observed spectroscopically, in which the benzimidazole is bound with too low an occupancy to be observed.

The position of 1,2-dimethylimidazole has been refined against the data, as this probe gives the clearest indication of its occupation and orientation within the artificial cavity of W191G. In addition, we have solved the structure of the

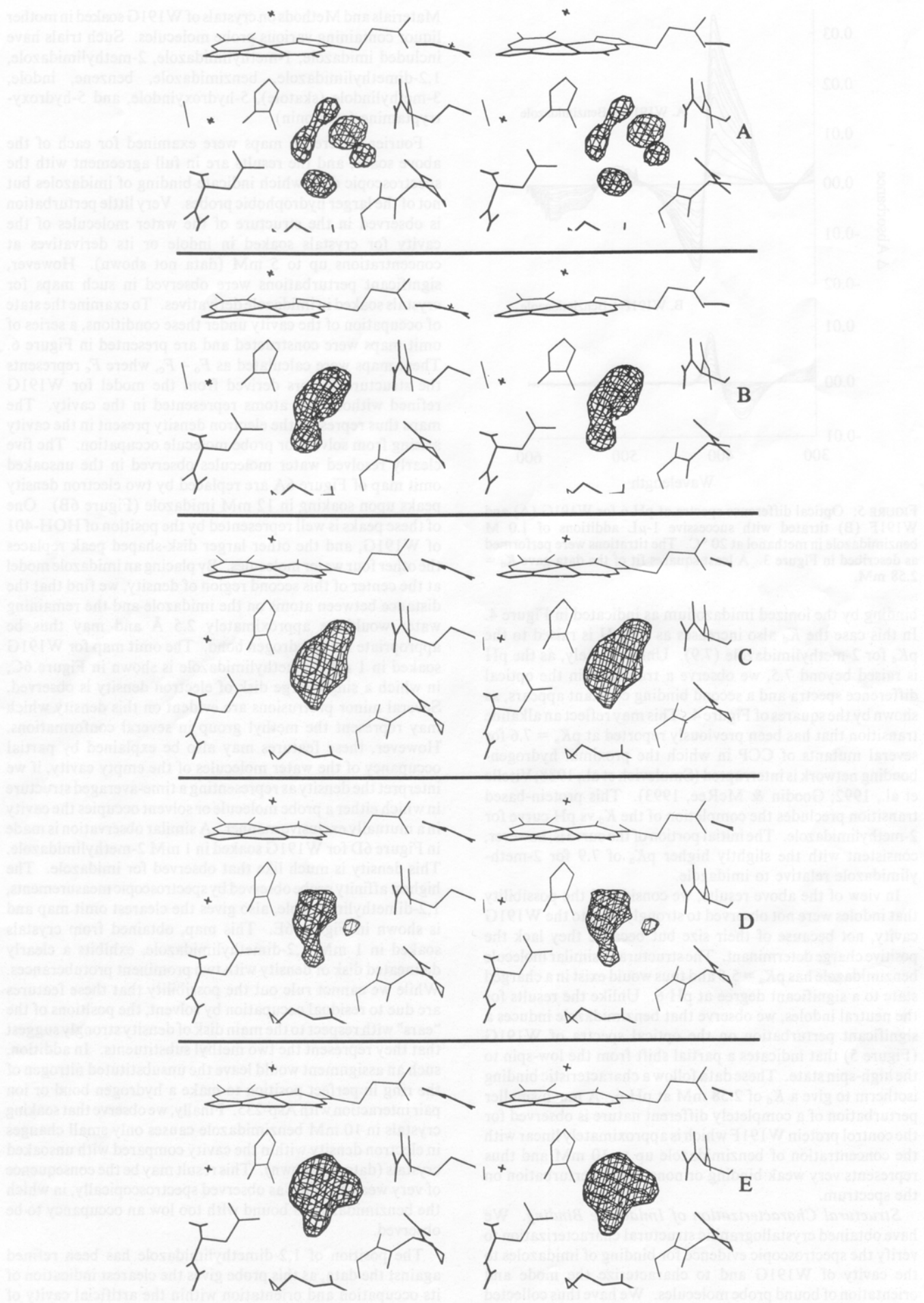


**FIGURE 6:** Stereoviews showing the Fourier omit maps for W191G and for crystals soaked in imidazole derivatives. Crystals were soaked in artificial mother liquor containing the indicated concentration of imidazole for 12 h prior to data collection. Omit maps were calculated as  $F_0 - F_c$ , where the calculated structure factors were derived from a model for W191G which had been refined without containing water or imidazole in the cavity. All maps are shown contoured at  $4\sigma$ . Panels: (A) W191G in the yeast crystal form; (B) W191G soaked in 12 mM imidazole; (C) 1 mM 1-methylimidazole; (D) 1 mM 2-methylimidazole; (E) 1 mM 1,2-dimethylimidazole.

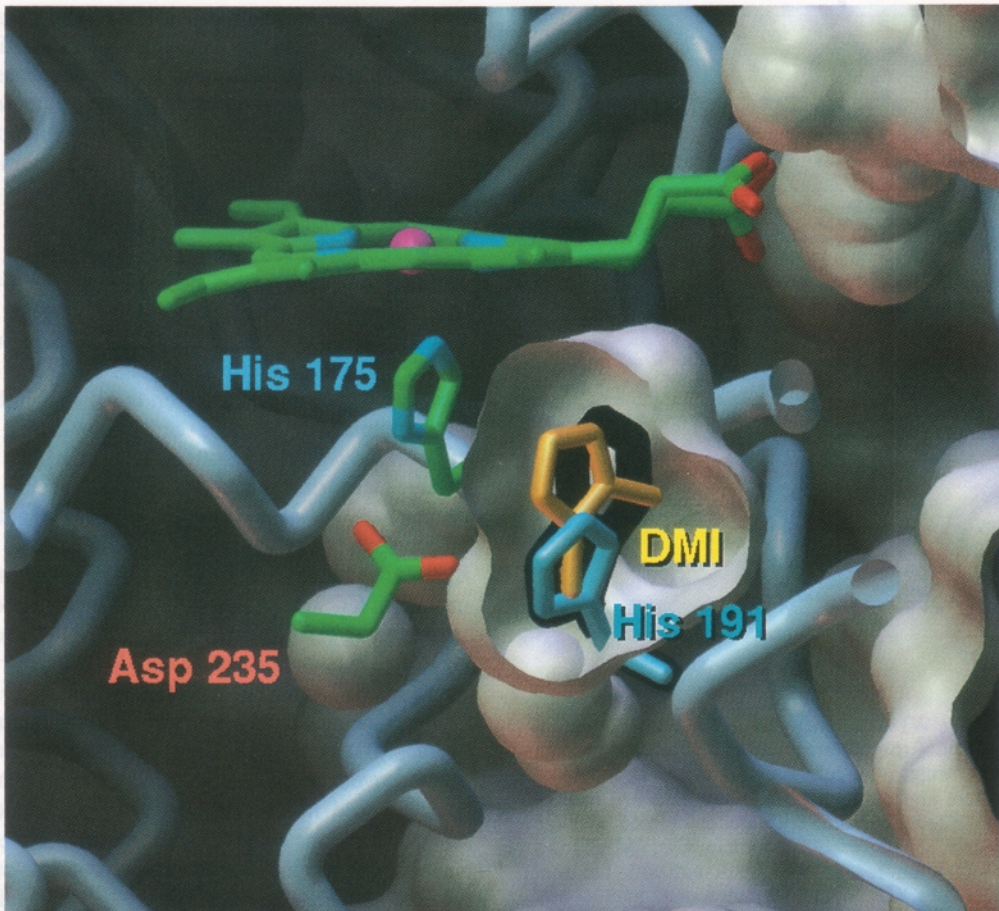


**FIGURE 7:** Cutaway view of the W191G cavity (gray) showing the relative positions of Trp-191 in the wild-type enzyme (black), His-191 in the 2.0-Å structure of the W191H mutant (blue), and the refined position of 1,2-dimethylimidazole bound to W191G (yellow). Also shown are the positions of the heme, His-175, and Asp-235, the latter of which is observed to make hydrogen bonds to each of the three occupants of this cavity. The cavity surface was calculated using a 1.4-Å probe sphere (Connolly, 1983).

W191H mutant to 2.0-Å resolution ( $R = 0.18$ ), in order to compare the relative positions of the imidazole rings. As shown in Figure 7, the refined position of the imidazole of His-191 lies almost exactly over the five-membered portion of the Trp-191 ring in the wild-type enzyme. The probe molecule 1,2-dimethylimidazole is observed to occupy a position that more fully occupies the center of the cavity but remains in a position ideal for making a hydrogen bond to Asp-235. A similar hydrogen bond is observed between Trp-191 of CCP(MKT) or His-191 of W191H and the carboxylate. This interaction is thus important in defining the orientation of the probe imidazoles and, in addition, is clearly critical in defining the determinant for positively charged molecules at this site.

**Effects of the Cavity on Function and Stability.** We have examined the functional properties and stability of W191G to determine the potential for utilizing this species as a functional oxidase for non-native substrates. W191G is observed at pH 6 to be in a six-coordinate low-spin species characterized by absorbance features at 412, 540, and 570 nm. This species nevertheless reacts with  $H_2O_2$  to provide a relatively stable product with absorption bands at 414, 530, and 560 nm, characteristic of ferryl hemes (Yonetani & Ray, 1965). This species decays with a  $t_{1/2}$  of approximately 400 s, which is of the same order as that of the ferryl center of

CCP(MKT) (Erman et al., 1992). However, as has been observed for W191F, the above mutants are essentially inactive with respect to cytochrome *c* (cyt *c*) oxidation. For example, the rate of cyt *c* oxidation by W191G at pH 6.0, in 20 mM Tris/phosphate buffer, at 22 °C was less than 0.2% of the rate observed for CCP(MKT). Equilibrium of W191G with imidazole derivatives at 12 μM or benzimidazole at 80 μM prior to reaction with  $H_2O_2$  did not effect the activity of W191G toward cyt *c* oxidation. In addition,  $H_2O_2$  oxidation of W191H alone or W191G in the presence of imidazoles did not result in the observation of EPR signals at 10 K that might result from the oxidation of these species. The inability to observe an imidazole radical bound to W191G is consistent with the report that ferrous W191H binds dioxygen but does not convert to an oxyferryl form (Miller et al., 1992), while the  $Fe^{2+}-O_2$  complex of native CCP transiently forms an oxyferryl product with the spectral properties of compound ES. It appears that intramolecular transfer to bound dioxygen occurs from Trp-191 but not from His-191.

The cavity introduced by W191G appears to significantly destabilize the protein toward thermal denaturation, while imidazole binding to the cavity partially reverses this destabilization. Below 37 °C, the optical spectra of these proteins displayed a gradual, approximately linear change as a function

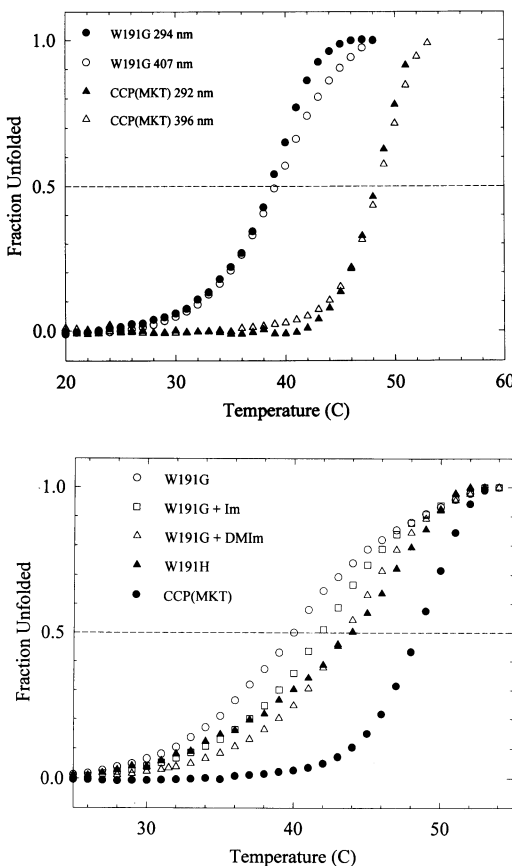


FIGURE 8: Effect of the W191G cavity and its state of occupation on the thermal stability of the protein. Optical difference spectra were collected as the sample temperature was raised at a rate of 2°/min. Samples were approximately 10 μM protein in 100 mM KP<sub>i</sub>, pH 6.0. (A, top) The unfolded fraction was calculated from the absorbance difference at 396 (Δ) or 292 (▲) nm for CCP(MKT) and at 407 (○) or 294 (●) nm for W191G. (B, bottom) Thermal denaturation profiles for CCP(MKT) (●) measured at 396 nm, W191G (○) at 410 nm, W191G in the presence of 5 mM imidazole (□) at 410 nm, W191G in the presence of 0.5 mM 1,2-dimethylimidazole (△) at 411 nm, and W191H (▲) measured at 360 nm.

of temperature and displayed several isosbestic points. Above 37 °C, a second transition occurred that preceded the irreversible unfolding of the proteins at about 57 °C. This second transition is shown in Figure 8A for CCP(MKT) and W191G at wavelengths in the Soret and in the UV region, with the wavelengths chosen at the isosbestic points for the first spectral transition.  $T_m$  values of 38.6 and 48.6 °C were observed for W191G and CCP(MKT), respectively. The absolute  $T_m$  values obtained are expected to depend upon conditions such as temperature scan rate, because the unfolding of CCP is only partially reversible (Gross & Erman, 1985). Nevertheless, the W191G cavity decreases the  $T_m$  by 10° relative to wild-type enzyme, and this difference is very similar to those observed in a number of artificial cavity mutants of T4 lysozyme (Eriksson et al., 1993). As shown in Figure 8B, the thermal denaturation profiles of W191G in the presence of imidazole or 1,2-dimethylimidazole result in  $T_m$  values which are intermediate between the wild-type enzyme and W191G in the empty state. This intermediate  $T_m$  behavior is also reproduced by the W191H mutant, again demonstrating its utility as a control for a fully occupied covalent "imidazole" bound state. These results are remarkably similar to the stabilization induced by benzene on T4 lysozyme cavity mutants (Eriksson et al., 1992a).

## DISCUSSION

Although large cavities are rarely observed in natural proteins, it has been recently shown that such cavities may be created by replacing buried hydrophobic residues of T4 lysozyme with smaller side chains (Eriksson et al., 1992a,b, 1993). These results have provided significant new insights into the importance of hydrophobic interactions and protein stability. They also suggest interesting possibilities for the usefulness of such structures in protein engineering. In this study we have characterized a cavity which has been created not just at the active site of an oxidative heme enzyme but in place of an amino acid which is efficiently oxidized by the native protein.

**The Uncollapsed Nature of the Cavity.** A number of mutants have previously been reported in T4 lysozyme that have resulted in buried cavities varying in size, depending upon the size of the replaced residue, the presence of preexisting cavities in the structure, and the degree of collapse of the surrounding protein (Eriksson et al., 1992a,b, 1993). Thus, cavities appear to be quite readily introduced into the interior of proteins without resulting in a complete collapse of the protein structure around the site. Such collapse would presumably result in destroying favorable interactions in the folded structure that would not be recovered by repacking of the internal defect. Even so, it is noteworthy that the W191G mutant of CCP results in essentially no collapse of the structure surrounding the site. However, three features of the protein structure may provide some insight into this result. First, the cavity walls would be expected to be quite rigid in this case as they are made up primarily of main-chain atoms. There are essentially no side chains in contact with Trp-191 that could move into the cavity space, so that any repacking of the cavity would necessarily involve significant movements in several portions of the peptide backbone conformation. Second, the "ceiling" of the cavity consists of the rigid heme macrocycle, adding significantly to the mechanical stability of the structure surrounding the site. Finally, the clearly observed occupation of the cavity with several ordered water molecules indicates that the cavity may be considered an additional region of the protein–solvent interface.

**Solvent Occupation of the Cavity.** The observation of ordered solvent in W191G is significant because of the fact that the cavity-forming mutants of T4 lysozyme were observed to show no evidence of such occupation (Eriksson et al., 1992a,b, 1993). Although lysozyme cavities have been characterized that are both larger and smaller than that observed for W191G, the T4 lysozyme cavities were introduced at very hydrophobic sites in the protein interior. In contrast, the cavity interface for W191G is quite polar and is composed of several peptide carbonyl oxygens and, most significantly, Asp-235. Specific interactions between solvent and these sites are clearly indicated. These interactions in the polar cavity may serve to order solvent that may otherwise be present but disordered.

**Small Molecule Binding to the Cavity.** The observed binding of alkylimidazole derivatives to the cavity of W191G may provide certain insights into the potential for creating "substrate" binding sites into proteins with defined specificity. As with the T4 lysozyme mutants, ready access to the buried cavity even in the crystalline state indicates a significant dynamic "breathing" of the structure (Eriksson et al., 1992a). In the case of W191G, binding affinity appears to be controlled by a combination of a positively charged molecule and the efficient filling of the cavity space. The positive charge determinant appears to be due to an ion pair interaction

between the imidazolium cation and the carboxylate of Asp-235. This conclusion is fully supported by the pH dependence of imidazole binding and by the interpretation of the electron density for 1,2-dimethylimidazole binding in which the orientation of the proposed methyl substituents indicates interaction of the imidazole NH with Asp-235. Thus, while it is not certain from the crystal structure to what extent unsubstituted imidazole undergoes free rotation about the axis normal to its plane, the data for 1,2-dimethylimidazole are at least consistent with an ordered occupation. It is also useful to compare the position of the imidazole with the position of the imidazole ring of the W191H mutant. In this case, the positions are similar, but the free imidazole is observed to more efficiently occupy the cavity volume than is allowed by the tethered imidazole of W191H. However, both of these forms are oriented so that either hydrogen-bonding or ion pair interaction is possible between the imidazole NH and Asp-235. Thus, examination of the binding properties of neutral hydrophilic molecules as well as other charged species on both the W191G protein and mutants in which the Asp-235 residue has been replaced by other amino acids will be of considerable interest. These studies are in progress.

The reason for the optimal affinity of 1,2-dimethylimidazole for binding to W191G is also readily apparent. It is possible that the methyl-substituted imidazoles bind better than unsubstituted imidazole due to the fact that their higher  $pK_a$  values result in a higher effective concentration of the charged species. However, the pH dependence of Figure 4 indicates that, even in the fully charged state, 1,2-dimethylimidazole has a lower  $K_d$  than that of imidazole. Thus it is most likely that the efficiency of filling the cavity with the appropriately sized molecule is the cause of this substituent effect. This would be expected due to the increased entropy that is gained from transfer of the methylimidazoles from solvent into the cavity. For 2-ethylimidazole, which also has a  $pK_a$  similar to that of the 2-methyl derivatives yet binds with a significantly increased  $K_d$ , it appears that the optimum size of the substituent has been exceeded.

The binding properties of indole and its derivatives were of considerable interest to our initial characterization of the cavity. Due to the lack of collapse of the cavity, and the complementarity of the cavity dimensions, it is not completely clear why binding of indole to W191G does not readily occur. Similar results were observed with a phenylalanine mutant of T4 lysozyme in which benzene did not bind to the cavity, even though it was observed to bind to cavities formed by replacement of a leucine (Eriksson et al., 1992a). In this case, however, some collapse of the cavity was observed, providing a reasonable explanation. We have considered that the negative results with indoles are the result of a hindered kinetic access of the larger probe to the buried cavity. However, several attempts at reconstituting the apo-W191G protein with heme in the presence of indole or its derivatives have not produced conclusive evidence for binding. Benzimidazole, with a  $pK_a = 5.5$ , does show evidence for weak binding to W191G in solution by its effect on the heme optical spectra. However, soaking crystals in 10 mM benzimidazole results in only small changes in the electron density for water molecules in the cavity. Thus, it is possible that benzimidazole may weakly bind to the cavity in solution but be present with too low an occupancy to be observed in the crystal structure. This would imply that the binding affinity is lower in the crystal than in solution, as the concentration of benzimidazole in the soak is severalfold higher than the  $K_d$  in solution. Studies

with substituted benzimidazoles with altered  $pK_a$  values are in progress to further characterize this behavior.

It is possible that indole is not stabilized in the cavity because it is not positively charged. This apparently paradoxical result may illustrate a significant insight into the function of the native enzyme. We have demonstrated that a positive charge is a determinant for the favorable interaction of probe molecules within the cavity created by removing the Trp-191 radical center. It is likely that the interaction between Asp-235 and these probes is the structural basis for this effect. We have recently demonstrated conclusively that the Trp-191 radical of the ES complex exists as the cation form of the radical (Sivaraja et al., 1989; Houseman et al., 1993) and that Asp-235 is important to the structural and functional integrity of the enzyme (Goodin & McRee, 1993). In a manner entirely analogous to the results in this work, the interaction between the Asp and Trp may stabilize the developing charge of the cation radical and be responsible for the remarkable stability of the Trp-191 cation free radical of the ES state.

#### ACKNOWLEDGMENT

We thank Mike Pique for computer graphics. In addition, we acknowledge Prof. B. W. Mathews, Prof. T. L. Poulos, Prof. B. M. Hoffman, Prof. J. A. Roe, Dr. G. M. Jensen, S. Wilcox, and S. M. Redford for stimulating discussions and critical comments.

#### REFERENCES

- Ator, M. A., & Ortiz de Montellano, P. R. (1987) *J. Biol. Chem.* 262, 1542.
- Ator, M. A., David, S. K., & Ortiz de Montellano, P. R. (1987) *J. Biol. Chem.* 262, 14954.
- Banci, L., Bertini, I., Bini, T. Z., Tien, M., & Turano, P. (1993) *Biochemistry* 32, 5825.
- Bredt, D. S., Hwang, P. M., Glatt, C. E., Lowenstein, C., Reed, R. R., & Snyder, S. H. (1991) *Nature* 351, 714.
- Brünger, A. T., Kuriyan, J., & Karplus, M. (1987) *Science* 235, 458.
- Clackson, T., & Winter, G. (1989) *Nucleic Acids Res.* 17, 10163.
- Connolly, M. L. (1983) *Science* 221, 709.
- Dawson, J. H. (1988) *Science* 240, 433.
- Depillis, G. D., Sishta, B. P., Mauk, A. G., & Ortiz de Montellano, P. R. (1991) *J. Biol. Chem.* 266, 19334.
- Dolphin, D., Forman, A., Borg, D. C., Fajer, J., & Felton, R. H. (1971) *Proc. Natl. Acad. Sci. U.S.A.* 68, 614.
- Eriksson, A. E., Baase, W. A., Wozniak, J. A., & Matthews, B. W. (1992a) *Nature* 355, 371.
- Eriksson, A. E., Baase, W. A., Zhang, X. J., Heinz, D. W., Blaber, M., Baldwin, E. P., & Matthews, B. W. (1992b) *Science* 255, 178.
- Eriksson, A. E., Baase, W. A., & Matthews, B. W. (1993) *J. Mol. Biol.* 229, 747.
- Erman, J. E., Vitello, L. B., Mauro, J. M., & Kraut, J. (1989) *Biochemistry* 28, 7992.
- Erman, J. E., Vitello, L. B., Miller, M. A., & Kraut, J. (1992) *J. Am. Chem. Soc.* 114, 6592.
- Finzel, B. C., Poulos, T. L., & Kraut, J. (1984) *J. Biol. Chem.* 259, 13027.
- George, P. (1952) *Nature* 169, 612.
- George, P. (1953) *Biochem. J.* 54, 267.
- Goodin, D. B., & Mcree, D. E. (1993) *Biochemistry* 32, 3313.
- Goodin, D. B., Mauk, A. G., & Smith, M. (1987) *J. Biol. Chem.* 262, 7719.
- Goodin, D. B., Davidson, M. G., Roe, J. A., Mauk, A. G., & Smith, M. (1991) *Biochemistry* 30, 4953.
- Gross, M. T., & Erman, J. E. (1985) *Biochim. Biophys. Acta* 830, 140.

- Houseman, A. L. P., Doan, P. E., Goodin, D. B., & Hoffman, B. M. (1993) *Biochemistry* 32, 4430.
- Kaput, J., Goltz, S., & Blobel, G. (1982) *J. Biol. Chem.* 257, 15054.
- Katritzky, A. R., & Rees, C. W. (1984) *Comprehensive Heterocyclic Chemistry*, Vol. 4, Pergamon, Oxford.
- Knowles, J. R. (1987) *Science* 236, 1252.
- Kunkel, T. A., Bebenek, K., & McClary, J. (1991) *Methods Enzymol.* 204, 125.
- Kwon, N. S., Nathan, C. F., Gilker, C., Griffith, O. W., Matthews, D. E., & Stuehr, D. J. (1990) *J. Biol. Chem.* 265, 13442.
- Leone, A. M., Palmer, R. M., Knowles, R. G., Francis, P. L., Ashton, D. S., & Moncada, S. (1991) *J. Biol. Chem.* 266, 23790.
- McRee, D. E. (1992) *J. Mol. Graphics* 10, 44.
- Miller, M. A., Bandyopadhyay, D., Mauro, J. M., Traylor, T. G., & Kraut, J. (1992) *Biochemistry* 31, 2789.
- Ner, S. S., Goodin, D. B., Pielak, G. J., & Smith, M. (1988a) *BioTechniques* 6, 408.
- Ner, S. S., Goodin, D. B., & Smith, M. (1988b) *DNA* 7, 127.
- Nicola, N. A., Minasian, E., Appleby, C. A., & Leach, S. J. (1975) *Biochemistry* 14, 5141.
- Ortiz de Montellano, P. R. (1986) in *Cytochrome P450* (Ortiz de Montellano, P. R., Ed.) Plenum, New York.
- Ortiz de Montellano, P. R. (1987) *Acc. Chem. Res.* 20, 289.
- Ortiz de Montellano, P. R. (1992) *Annu. Rev. Pharmacol. Toxicol.* 32, 89.
- Sakurada, J., Takahashi, S., & Hosoya, T. (1986) *J. Biol. Chem.* 261, 9657.
- Saunders, B. C. (1973) in *Inorganic Biochemistry* (Eichhorn, G. L., Ed.) Vol. 2, p 988, Elsevier, Amsterdam.
- Scholes, C. P., Liu, Y., Fishel, L. A., Farnum, M. F., Mauro, J. M., & Kraut, J. (1989) *Isr. J. Chem.* 29, 85.
- Sivaraja, M., Goodin, D. B., Smith, M., & Hoffman, B. M. (1989) *Science* 245, 738.
- Smulevich, G., Mauro, J. M., Fishel, L. A., English, A. M., Kraut, J., & Spiro, T. G. (1988) *Biochemistry* 27, 5477.
- Studier, F. W., Rosenberg, A. H., Dunn, J. J., & Dubendorff, J. W. (1990) *Methods Enzymol.* 185, 60.
- Thanabal, V., De Ropp, J. S., & La Mar, G. N. (1987) *J. Am. Chem. Soc.* 109, 7516.
- Tien, M., & Kirk, T. K. (1983) *Science* 221, 661.
- Veitch, N. C., & Williams, R. J. P. (1990) *Eur. J. Biochem.* 189, 351.
- Vitello, L. B., Erman, J. E., Miller, M. A., Mauro, J. M., & Kraut, J. (1992) *Biochemistry* 31, 11524.
- Wang, J. M., Mauro, J. M., Edwards, S. L., Oatley, S. J., Fishel, L. A., Ashford, V. A., Xuong, N. H., & Kraut, J. (1990) *Biochemistry* 29, 7160.
- Wells, T. N. C., & Fersht, A. R. (1985) *Nature* 316, 656.
- White, K. A., & Marletta, M. A. (1992) *Biochemistry* 31, 6627.
- Yonetani, T., & Ray, G. S. (1965) *J. Biol. Chem.* 240, 4503.
- Yonetani, T., Schleyer, H., & Ehrenberg, A. (1966) *J. Biol. Chem.* 241, 3240.